Structure and electronic properties of the orthorhombic MoRuP superconductor prepared at high pressure

W. Wong-Ng,[1] W. Y. Ching,[2] Yong-Nian Xu,[2] J. A. Kaduk,[3] I. Shirotani,[4] and L. Swartzendruber[1]
[1]*Materials Science and Engineering Laboratory, National Institute of Standards and Technology, Gaithersburg, Maryland 20899*
[2]*Department of Physics, University of Missouri–Kansas City, Kansas City, Missouri 64110*
[3]*British Petroleum Chemicals, P.O. Box 3011 MC F-9, Naperville, Illinois 60566*
[4]*Muroran Institute of Technology, 27-1, Mizumoto, Muroran-shi 050-8585, Japan*
(Received 3 July 2002; revised manuscript received 27 December 2002; published 30 April 2003)

The orthorhombic superconductor MoRuP (*o*-MoRuP) was prepared under high pressure, and its structure was refined using the x-ray Rietveld technique. The grayish-black sample of *o*-MoRuP is a superconductor with $T_c = 15.5$ K and having space group *Pnma* and lattice parameters $a = 6.03503(16)$ Å, $b = 3.85311(8)$ Å, and $c = 6.94355(17)$ Å, $V = 161.463(7)$ Å.[3] The structure of *o*-MoRuP is characterized by layers (parallel to the *ac* plane) of Mo, Ru, and P atoms. Based on the accurately determined crystal structure, the band structure and the density of states (DOS) of *o*-MoRuP were calculated by a first-principles density-functional method and compared with those of the isostructural superconductor *o*-ZrRuP ($T_c = 4$ K). It is shown that the high T_c in *o*-MoRuP is directly related to the higher level of the DOS at the Fermi level (E_F) and is traced to be predominantly from the Mo $4d$ orbitals. The calculated values of the DOS at E_F are 0.46 and 0.33 states/eV atom for the Mo and Zr analogs, respectively. The electronic bonding in these two crystals is analyzed in terms of the Mulliken effective charge and the bond order values. The bonding in *o*-MoRuP differs from that in *o*-ZrRuP in that there is a short (2.44 Å) Mo-P bond. The x-ray reference pattern of *o*-MoRuP prepared using a Rietveld decomposition technique has been submitted to the International Center for Diffraction Data to be included in the Powder Diffraction File.

DOI: 10.1103/PhysRevB.67.144523 PACS number(s): 74.10.+v, 74.70.Ad, 74.62.Bf

I. INTRODUCTION

Various ternary transition compounds with chemical formula of $TT'X$ (where X represents Si, Ge, and P and where T and T' represent $3d$, $4d$, and $5d$ transition metals) have been investigated since the 1960s.[1–11] In $TT'X$, T is conventionally to the left of T' in the periodic table. In recent years, the phosphides and silicides received increased attention because of the interesting superconductivity properties.[12–18]

There are two structure types for $TT'X$, both of which are layer structures. The first structure type is hexagonal $P\bar{6}m2$ (Fe_2P type). Representative examples are MRuP (M = Ti,Zr,Hf,Mn), MOsP (M = Ti,Zr,Hf), MNiP (M = Mn,Fe,Co,Mo,W), MRhP (M = Cr,Mn), CrPdP, and CaAgP.[1–7] The second structure type is referred to as the anti-$PbCl_2$ type (or Co_2Si), which has the orthorhombic space group *Pnma*. Examples are TiRuP, TiPdSi, MnRhSi, ZrFeGe, ZrRhGe, and NbRhGe.[4,11–15] The orthorhombic phase transforms to the higher-symmetry hexagonal form at high temperatures and pressures.[8] We will refer these two phases as *o*-$TT'X$ and *h*-$TT'X$, respectively.

As the powder x-ray diffraction technique is of primary importance for phase characterization, extensive coverage and accurate reference diffraction patterns of the superconductor and related phases in the Powder Diffraction File[19] (PDF) are essential for the superconductivity research community. Furthermore, accurately determined crystal structure including the atomic positions enables theoretical calculations of the electronic structure. A goal of this investigation is to supplement the reference diffraction patterns and crystal structures of *o*-MoRuP by using the x-ray Rietveld method.[20–22] In addition, the electronic structure of *o*-MoRuP is calculated and compared to isostructural *o*-ZrRuP in order to explain the significant difference in their superconducting temperatures. Past investigations on the superconducting properties of the $TT'X$ alloys seem to indicate that those alloys having T_c above 10 K tend to be in the *h*-$TT'X$ group. Alloys in the orthorhombic phase generally have lower T_c of less than 5 K. Arguments had been made that this is probably due to the different layered structures in the hexagonal and orthorhombic phases that resulted in different *T*-*T* and *T'*-*T'* connectivity.[10] It is therefore significant that the new *o*-MoRuP can have T_c as high as 15.5 K.[17,18] A sound explanation of this difference requires detailed information on the electronic structures of these alloys, which is the second goal of this investigation. In the past, most of the explanation for the difference in T_c in $TT'X$ alloys was based on indirect evidence such as the number of electrons per crystal and the Mo-Mo interatomic bond distances, etc.[17,18] To our knowledge, no rigorous *ab initio* calculations of the band structures of these crystals have been performed. Seo *et al.* had calculated electronic structure of *h*-ZrRuP, *o*-ZrRuP, and *h*-ZrRuSi using extended Hückel method,[23] which is of limited accuracy. In this paper, we present the results of first-principles calculations of the electronic structure of *o*-MoRuP based on the newly refined structure. A similar calculation on *o*-ZrRuP ($T_c \sim 4$ K) is also carried out using the structure determined by Muller *et al.*[10] By comparing the results of these two crystals, we can delineate the subtle difference in the structure and bonding of the two crystals, identify the factors that lead to the differences in T_c, and shed some light on the nature of superconductivity in the $TT'X$ alloys in general.

The paper is organized as follows. We first describe the experimental determination of the crystal structure in Sec. II. The results of theoretical calculations are presented in Sec. III. Finally, a brief section on comments and perspectives is given in the last section.

II. EXPERIMENT (REF. 37)

A. Sample preparation and superconductivity measurements

The preparation of the *o*-MoRuP sample at high temperature and pressure has been presented before.[17] A wedge-type cubic anvil high-pressure apparatus was used. The sample assembly for the preparation of the compounds is similar to that of the synthesis of black phosphorus.[24] The starting materials were placed into a crucible made of boron nitride (BN) and with the graphite heater was inserted into the pyrophyllite cube. The *o*-MoRuP sample was prepared by reaction of stoichiometric amounts of the powders of Mo, Ru, and P at a pressure around 4 GPa. The reactions were carried out at a temperature between 1200 and 1700 °C.

Superconductivity measurements were conducted using a superconducting quantum interference device (SQUID) magnetometer. The sample was cooled from 100 to 2 K in an applied field of 800 A/m (10 Oe) and some of these results have been reported previously.[17,18]

B. X-ray Rietveld refinements

For the x-ray diffraction measurement, the *o*-MoRhP powder was mounted in a zero-background quartz holder with double-sided adhesive tape. A Scintag PAD V diffractometer equipped with an Ortec intrinsic Ge detector was used to measure the powder patterns (Cu $K\alpha$ radiation, 40 kV, 30 mA) from 3° to 140° 2θ in 0.02° steps, counting for 10 s per step. All data processing and Rietveld structural refinements[20,21] were carried out using the General Structure Analysis System.[22] The reported structure[13] of *o*-ZrRuP was employed as a starting model for refinement. Included in the refinements were the atomic coordinates (with fixed isotropic displacement coefficients), a scale factor, a sample displacement coefficient, and the lattice parameters of the orthorhombic MoRuP. The peak profiles were described using a Thompson-Cox-Hastings pseudo-Voigt function with the ''finger'' asymmetry parametrization and the ''Stephens'' treatment of anisotropic strain broadening (profile function no. 4); in the final refinement, only the Gaussian *U* (strain), the Cauchy *X* (size), and the specimen displacement coefficients were refined. The background was described using a six-term cosine Fourier series. The small degree of preferred orientation was described using second-order symmetrized spherical harmonics. The 26.6°–27.1° 2θ region (which contained a peak from an unidentified impurity) was excluded from the refinements.

The similarity of Mo and Ru (42 and 44 electrons, respectively) means that we would expect to use structural criteria to make the metal-atom-type assignments. The average Mo-P distance, obtained from an analysis of structures in the CRYSTMET database[25] is 2.48(7) Å, and the average Ru-P distance is 2.37(8) Å. The expected distances by the bond valence formalism[26] are 2.44 Å for Mo-P and 2.29 Å for Ru-P, a Ru-P bond is expected to be significantly shorter than a Mo-P bond. The refined bond distances led to the reported atom-type assignments, but in fact interchanging the Mo and Ru positions led to significantly higher refinement residuals ($\chi^2 \sim 4.36$).

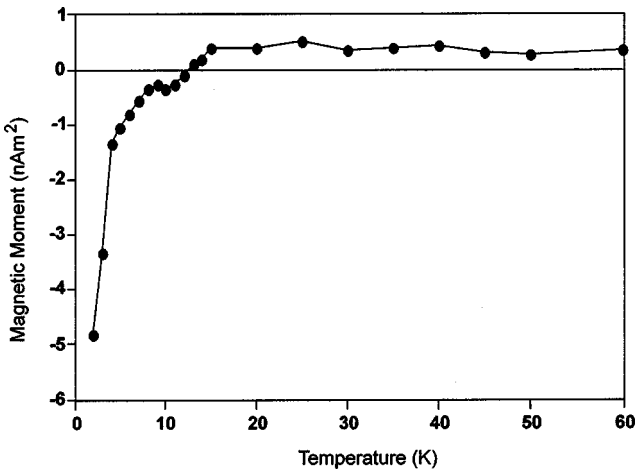

FIG. 1. A plot of the magnetic moment of *o*-MoRuP as a function of temperature.

The reference x-ray pattern of *o*-MoRuP was obtained with a Rietveld pattern decomposition technique. The pattern represents an ideal specimen pattern and was corrected for systematic errors both in the interplanar *d*-spacing values (*d*) and integrated intensity values of the diffraction peaks (*I*). The reported peak positions were calculated from the refined lattice parameters, as they represent the best measure of the true positions. For peaks resolved at the instrument resolution function, the individual peak positions are reported. For overlapping peaks, the intensity-weighted average peak position is reported with multiple indices. For marginally resolved peaks, individual peaks are reported to more accurately simulate the visual appearance of the pattern.

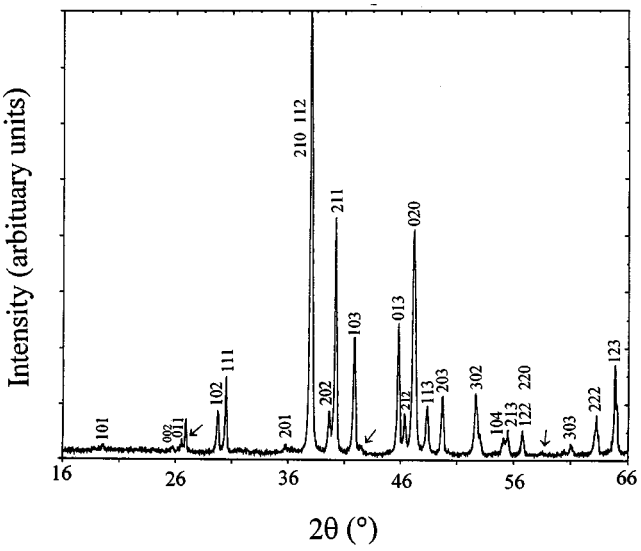

FIG. 2. X-ray powder diffraction pattern of *o*-MoRuP. Miller *hkl* indices are shown for the main orthorhombic phase.

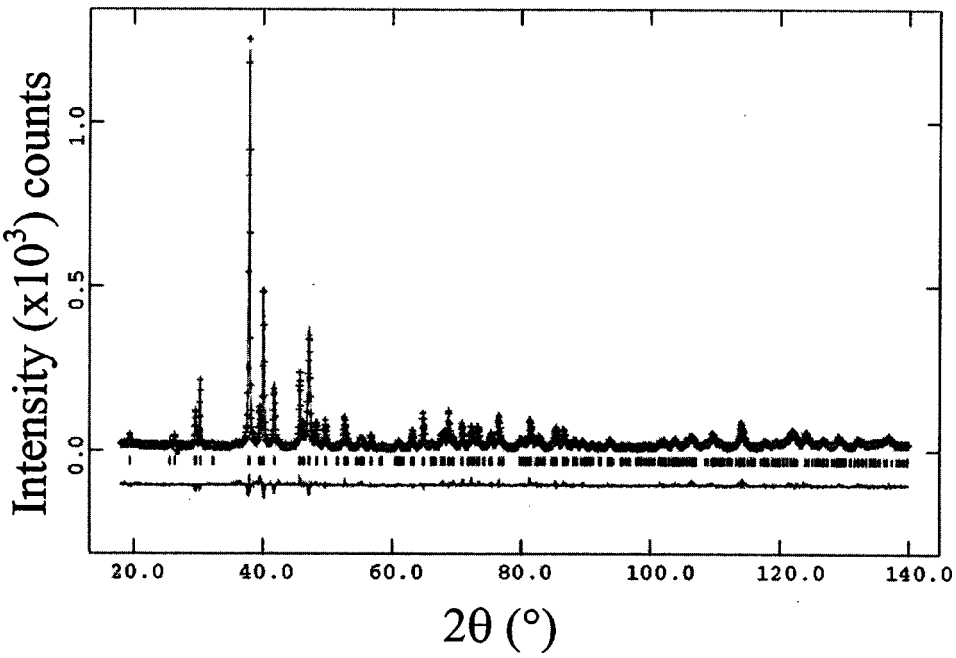

FIG. 3. Observed, calculated, and difference diffraction patterns of *o*-MoRuP. The small crosses represent the observed data points, and the smooth line through them the calculated pattern. The difference pattern is plotted at the same scale as the other patterns. The row of tick marks indicates the calculated peak positions.

C. Results and discussion

Figure 1 shows a plot of the magnetic moment of *o*-MoRuP as a function of temperature from 60 K down to 2 K. At high temperatures the sample is paramagnetic. At low temperatures the sample becomes diamagnetic due to the presence of superconductivity. The onset temperature, T_c, was observed at ~15 K as compared to the 4-K value reported for the *o*-ZrRuP.[14] This value agrees with that reported by Shirotani *et al.*[17]

The powder x-ray diffraction pattern of *o*-MoRuP along with the Miller *hkl* indices is shown in Fig. 2. Peaks that are marked with an arrow (at 2θ values of 26.9° and 42.4°) indicate the presence of a small amount of a second unidentified phase. *o*-MoRuP is confirmed to be isostructural to *o*-ZrRuP (Co_2Si structure type), which was characterized by Muller *et al.* using single-crystal x-ray diffraction methods.[10] The space group *Pnma* (No. 62) was chosen to conform to the standard setting. The final refinement of 21 variables using 6072 observations yielded the residuals $wRp=0.1062$, $Rp=0.0798$, $\chi^2=3.387$, $R(F^2)=0.0825$, and $R(F)=0.0584$; the slope and intercept of the normal probability plot were 1.708 and 0.125, respectively. These relatively large values arise principally from the granularity of the specimen and, to a smaller extent, the presence of a second minority phase. The agreement of the observed and calculated patterns is excellent (Fig. 3). The lattice parameters of *o*-MoRuP are listed in Table I along with those of the analogs *o*-ZrRuP and *o*-NbRuP. Table II gives the atomic coordinates of *o*-MoRuP.

Considering only the metal-phosphorus connectivity, the *o*-MoRuP structure is composed of edge-sharing RuP_4 tetrahedra [Fig. 4(a)] and MoP_5 square pyramids [Fig. 4(b)]. The P atoms are at the corner of these polyhedra and Mo and Ru are not shown. These two types of polyhedra fill the space of the structure. Since all atoms are positioned in layers parallel to the *ac* plane and are separated by a distance of *b*/2, *o*-MoRuP can also be viewed as having a two-dimensional layered structure. All layers are filled with Mo, Ru, and P and are equivalent to each other except with translation (Fig. 5). These layers consist of zigzag chains formed by triangular Mo-Ru-Mo clusters (or Zr-Ru-Zr clusters in *o*-ZrRuP) running parallel to the *a* direction (Fig. 6). P atoms were found in the spaces between the chains. As the metallic radius of Mo is smaller than Zr (1.40 vs 1.60 Å), the interatomic *M*-*M*, *M*-Ru, and *M*-P distances in the $M=$Zr analog are larger than those found in the compound with $M=$Mo (shown in Table III) as expected. It has been speculated that the two-dimensional planar framework of *T* and *T'* in the *TT'P* type structure may play an important role in the superconducting properties.[12–16] As will be shown later, a more detailed explanation must be based on accurate quantum-mechanical calculations of the electronic structure of these crystals.

The x-ray reference pattern of *o*-MoRuP (Fig. 3) was submitted to the International Center for Diffraction Data

TABLE I. Lattice parameters and superconducting transition temperatures $T_{c(\text{onset})}$ of the orthorhombic phosphides *M*RuP ($M=$Zr, Nb, and Mo).

Compound	*a* (Å)	*b* (Å)	*c* (Å)	*V* (Å^3)	$T_{c(\text{onset})}$ (K)	Reference
ZrRuP	6.4169(6)	3.8623(4)	7.3215(8)	181.46(3)	3.82	10
NbRuP	6.318(1)	3.719(1)	7.173(1)	168.5	<1.1	10
MoRuP	6.03503(16)	3.85311(8)	6.94355(17)	161.46	~15	This work

TABLE II. Atomic coordinates of MoRuP.

Atom	*x*	*y*	*z*	U_{iso}(Å^2)
Ru	0.1418(2)	1/4	0.4325(2)	0.001
Mo	0.0262(2)	1/4	0.8295(2)	0.001
P	0.7567(8)	1/4	0.3823(5)	0.005

(ICDD) to be included in the Powder Diffraction File (PDF). Table IV lists the x-ray diffraction pattern of *o*-MoRuP. In this table, the interplanar *d* spacings, Miller indices, and the integrated intensity values *I* are reported. The symbols *M* and + refer to peaks containing contributions from two and more than two reflections, respectively.

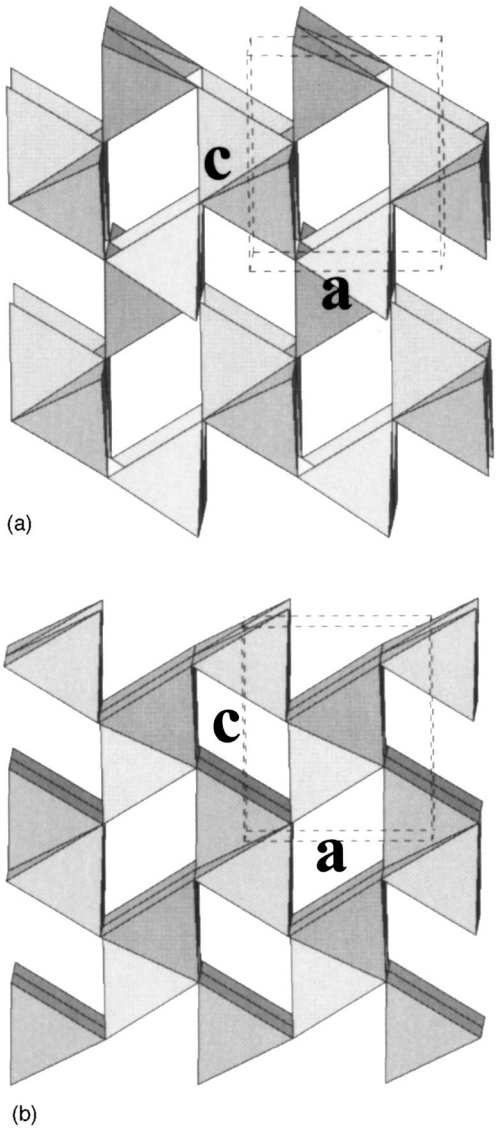

FIG. 4. Structure of *o*-MoRuP showing (a) the edge-sharing RuP_4 tetrahedra and (b) distorted MoP_5 square pyramids, both viewed approximately along the *b* axis.

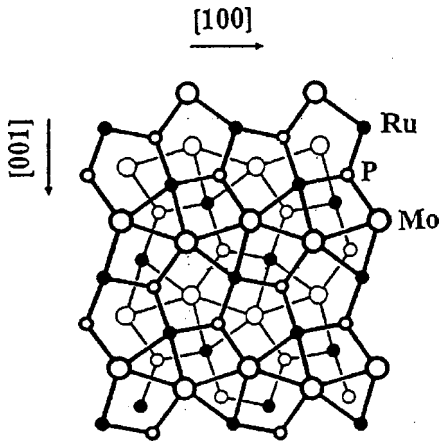

FIG. 5. Projection of the orthorhombic structure of MoRuP. Atoms connected by thick and thin lines are separated by half a translation period in the projection [010] direction.

III. ELECTRONIC STRUCTURE CALCULATION

A. Method of calculation

The electronic structure of the two isostructural superconductors *o*-MoRuP and *o*-ZrRuP were calculated using the orthogonalized linear combinations of atomic orbitals (OLCAO) method.[27] This is a density-functional-theory-based first-principles method, which has been used for electronic structures of many complex crystals, including one of the earliest calculations for the YBCO superconductor [28,29] and the alkali-doped C_{60}-based superconductor,[30,31] as well as the complex organic superconductors.[32,33] In the present calculation, the basis functions were expanded in atomic orbitals of Mo, Ru, Zr, (Kr[core], 5*s*, 6*s*, 5*p*, 6*p*, 4*d*, 5*d*), P ([Ne] core, 3*s*, 4*s*, 2*p*, 3*p*, 3*d*). The atomic orbitals were ex-

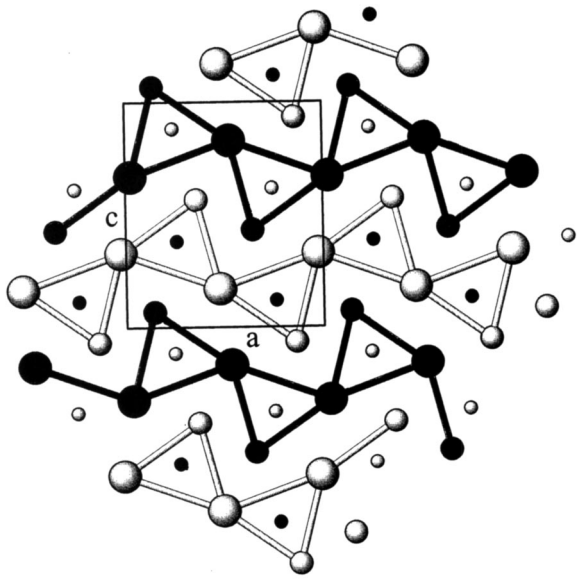

FIG. 6. Projection of the structure of orthorhombic *M*RuP (*M* = Mo and Zr), showing the one-dimensional *M*-Ru chains. Large spheres, *M*; medium size spheres, Ru; small spheres, P. Dark-colored spheres, $y=\frac{1}{4}$; light-colored spheres, $y=\frac{3}{4}$.

TABLE III. Interatomic distances (Å) for *o*-MoRuP and *o*-ZrRuP. Data for the Zr analog (Ref. 10) are included for comparison.

	Distance			Distance	
Atom-atom	$M=$Mo	$M=$Zr	Atom-atom	$M=$Mo	$M=$Zr
Ru-Ru	2.742(2)×2	2.874×2	Ru-P	2.350(5)	2.457
				2.293(4)	2.453
Ru-*M*	2.843(2)	2.903		2.396(2)×2	2.398×2
	2.870(1)×2	2.982×2			
	2.837(1)×2	2.926×2	*M*-*M*	3.069(2)×2	3.285×2
	2.848	2.967		3.213(1)×2	3.366×2
M-P	2.600(3)×2	2.746×2			
	2.755(3)×2	2.742×2			
	2.438(4)	2.740			

pressed in term of Gaussian-type orbitals (GTO's). The crystal potentials are written as superpositions of atom-centered functionals, also consisting of GTO's. The crystal potentials were iterated to full self-consistency when the total energy of the crystal converges to within 10^{-7} eV. 72 k points in the irreducible portion of the Brillouin zone (BZ) were used for the determination of the Fermi level E_F and for the evaluations of the density of state (DOS). Application of this method to geometry optimization by the total-energy minimization scheme shows that the maximum differences in the calculated and measured lattice constants are 1.3% for *o*-MoRuP, 0.8% for *o*-ZrRuP, and only 0.3% for *h*-ZrRuP, respectively.[34] This gives us great confidence in the computational method we adopted for the $TT'X$ superconductors.

B. Band structure and density of states

The band structure near the Fermi level for *o*-MoRuP and *o*-ZrRuP are shown in Figs. 7(a) and 7(b), respectively. MoRuP has two more conduction electrons in the unit cell than ZrRuP, which resulted in a significant difference in the band structures near E_F. *o*-MoRuP has more bands crossing E_F, thus creating a large number of electron and hole pockets at the Fermi surface and a higher number of DOS's at E_F, or $N(E_F)$. Two remarkable features for both crystals are observed. First, E_F is located at the top of the band at the zone center Γ; second, a significant number of band degeneracy and band crossing occur at the S point $[(\frac{1}{2},\frac{1}{2},0)\pi/a]$ of the BZ. In *o*-ZrRuP, this crossing is about 0.2 eV below E_F. In *o*-MoRuP, this crossing moves up, closer to E_F because of two additional $4d$ electrons per formula unit, resulting in a higher value of $N(E_F)$. Our calculated $N(E_F)$ for *o*-MoRuP and *o*-ZrRuP are 0.46 and 0.33 states per eV atom, respectively. The former is almost 40% larger. Our band structure of *o*-ZrRuP is completely different from those of Ref. 23 using the extended Hückel method. They found the opposite trend in $N(E_F)$ vs T_c in *o*-ZrRuP and *h*-ZrRuP. No hard

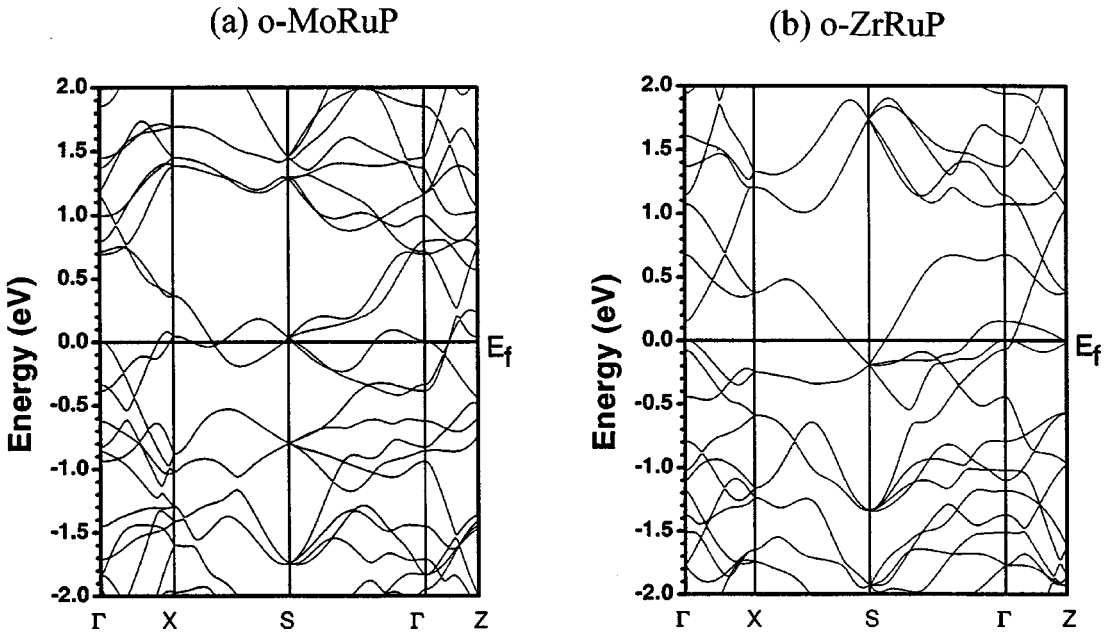

FIG. 7. Calculated band structure of (a) *o*-MoRuP and (b) *o*-ZrRuP. The Fermi level is at the energy 0 eV.

TABLE IV. X-ray diffraction pattern for *o*-MoRuP [*Pnma* with $a=6.03503(16)$ Å, $b=3.85311(8)$ Å and $c=6.94355(13)$ Å]. The interplanar *d* spacings, Miller indices, and the integrated intensity values *I* are given. Symbols *M* and + refer to peaks containing contributions from two and more than two reflections, respectively.

d	*I*	*h*	*k*	*l*	*d*	*I*	*h*	*k*	*l*	*d*	*I*	*h*	*k*	*l*
4.55507	19	1	0	1	3.47181	5	0	0	2	3.36908	40	0	1	1
3.01176	77	2	0	0*M*	3.01176	77	1	0	2*M*	2.94174	118	1	1	1
2.76754	6	2	0	1	2.37300	999	2	1	0*M*	2.37300	999	1	1	2*M*
2.27753	99	2	0	2	2.24778	407	2	1	1	2.16107	195	1	0	3
1.98408	206	0	1	3	1.96062	56	2	1	2	1.93226	161	3	0	1
1.92651	257	0	2	0	1.88484	77	1	1	3	1.83652	76	2	0	3
1.74062	75	3	0	2	1.73591	23	0	0	4	1.72723	26	3	1	1
1.66827	22	1	0	4	1.65783	20	2	1	3	1.62291	24	2	2	0*M*
1.62291	24	1	2	2*M*	1.51836	12	3	0	3	1.47439	13	4	0	1
1.47087	33	2	2	2	1.43805	104	1	2	3	1.41263	13	3	1	3
1.38377	41	4	0	2	1.37701	50	4	1	1	1.36428	116	3	2	1
1.35336	31	1	0	5	1.32929	68	2	2	3	1.30646	69	0	1	5
1.30233	20	4	1	2	1.29154	65	3	2	2	1.28961	21	0	2	4
1.26140	54	2	0	5*M*	1.26140	54	1	2	4*M*	1.24388	136	3	1	4
1.23614	8	1	3	1	1.20098	14	4	1	3	1.19892	21	2	1	5
1.19251	16	3	2	3	1.18920	5	5	0	1	1.18142	120	2	3	0*M*
1.18142	120	1	3	2*M*	1.17085	20	4	2	1	1.16500	50	2	3	1
1.13877	5	4	0	4	1.13634	88	1	0	6*M*	1.13634	88	5	1	1*M*
1.12389	40	4	2	2	1.12303	33	0	3	3	1.11872	8	2	3	2
1.10742	25	1	2	5	1.10407	10	1	3	3	1.09568	18	3	1	5
1.09324	6	5	1	2	1.09013	6	1	1	6	1.08053	12	2	0	6
1.05540	31	2	2	5	0.99547	15	6	0	1	0.99101	32	5	0	4
0.98064	17	3	3	3+	0.97886	29	1	2	6*M*	0.97886	29	1	0	7*M*
0.96843	21	4	3	1	0.96332	52	6	1	1*M*	0.96332	52	0	4	0*M*
0.96062	14	0	1	7	0.95977	22	5	1	4	0.94868	25	1	1	7
0.94264	74	0	3	5*M*	0.94264	74	2	2	6*M*	0.94135	10	4	3	2
0.93712	23	6	1	2	0.93557	6	5	2	3	0.92251	7	6	0	3
0.91848	130	3	3	4*M*	0.91848	130	4	0	6*M*	0.91740	6	1	4	2
0.91536	12	2	1	7	0.90087	9	4	3	3	0.90000	13	2	3	5
0.89324	19	4	1	6	0.89164	9	6	2	0	0.88717	12	2	4	2
0.88438	37	6	2	1	0.88125	85	5	2	4	0.87981	38	1	4	3
0.87261	98	1	2	7*M*	0.87261	98	5	3	1*M*	0.86795	10	0	0	8
0.86207	43	3	4	1	0.85378	18	3	3	5	0.85297	37	2	4	3*M*
0.85297	37	5	3	2*M*	0.85114	6	1	3	6	0.84281	35	3	4	2
0.84227	10	0	4	4	0.83852	8	1	1	8	0.83675	13	7	0	2
0.83417	17	1	4	4*M*	0.83417	17	2	0	8*M*	0.83204	20	6	2	3
0.82891	83	4	2	6*M*	0.82891	83	4	0	7*M*	0.82683	8	2	3	6
0.82220	10	5	3	3										

evidence of one-dimensional or two-dimensional features of the band structure are found in our calculation. However, the different layered structures in *o*-ZrRuP discussed in Sec. II C could have played some role in determining their respective electronic structures and special features near the Fermi surfaces.

The calculated total DOS and atom-resolved partial DOS (PDOS) of the two crystals are shown in Figs. 8 and 9. The higher value of $N(E_F)$ in *o*-MoRuP comes from the 4*d* orbitals of the Mo atom based on the inspection of the wave functions. The contributions from Ru to $N(E_F)$ in the two crystals are about the same while those from P are very small. In the BCS theory of metallic superconductivity, T_c is directly related to $N(E_F)$ and the electron-phonon coupling constant based on McMillan formula[35] is given by

$$T_c=[\langle\omega_{\log}\rangle/1.2]\exp\left[\frac{-1.04(1+\lambda)}{\lambda-\mu^*-0.62\lambda\mu^*}\right], \qquad (1)$$

where $\langle\omega_{\log}\rangle$ is the logarithmically averaged phonon frequency, μ^* is the renormalized Coulomb pseudopotential, and $\lambda=N(E_F)/V$ is the electron-phonon coupling constant,

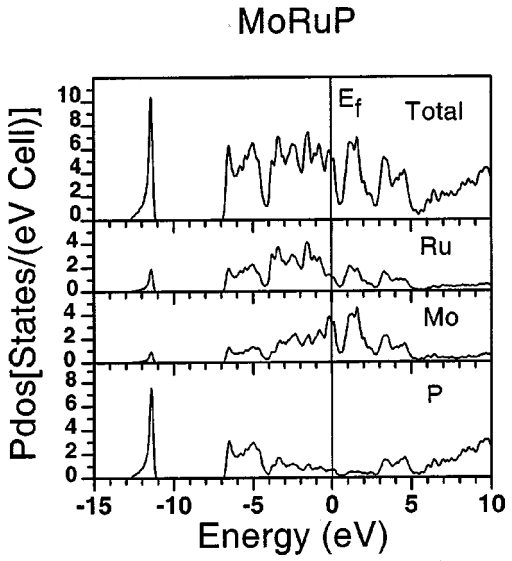

FIG. 8. Calculated total and partial DOS of *o*-MoRuP. (a) Total, (b) Ru, (c) Mo, and (d) P.

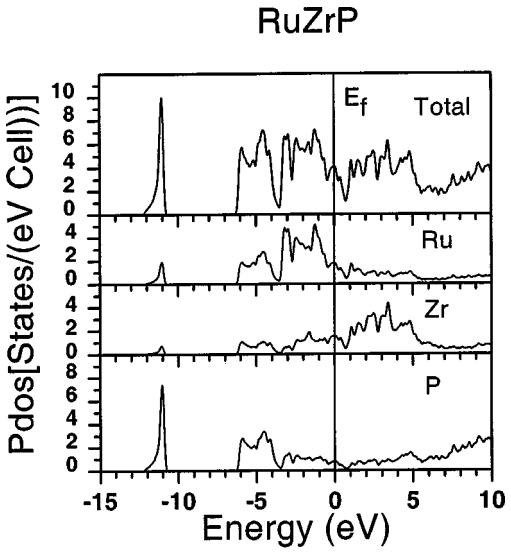

FIG. 9. Calculated total and partial DOS of *o*-ZrRuP. (a) Total, (b) Ru, (c) Zr, and (d) P.

where V stands for the electron-phonon coupling strength. A higher value of $N(E_F)$ can account for a higher T_c. Since *o*-MoRuP and *o*-ZrRuP are isostructural, it is not unreasonable to expect them to have similar lattice properties; it is therefore quite obvious that the difference in T_c can be readily explained by the difference in the $N(E_F)$ values and to a lesser extent, the complex features of the Fermi surface. Also, *o*-MoRuP has a larger bandwidth (6.9 eV) than *o*-ZrRuP (6.3 eV).

C. Electronic bonding in *o*-MoRuP

To understand the electronic bonding in these two crystals, the Mulliken effective charge Q^* and the bond order between metal and P and between metal and metal were calculated based on the Mulliken scheme.[36] A separate minimal basis set was used in these calculations. The results are listed in Tables V and VI. The calculated *M*, Ru, and P atomic charges are 5.751, 8.2758, and 4.974 for *o*-MoRuP and 3.330, 8.529, and 5.143 for *o*-ZrRuP. The charge transfers in these alloys are quite small, but the difference between the two crystals is evident. In *o*-MoRuP, Mo loses 0.25 electron to Ru and P loses only 0.03 electron. In *o*-ZrRuP, Zr loses 0.67 electron, mostly to Ru (0.53 electron) but also to P (0.14 electron). This difference in the charge transfer obviously affects the bonding in these two crystals with a concomitant change in their band structure near the Fermi level.

The calculated bond order (BO) values are listed in Table VI. The corresponding bond distances are listed in Table III. The smaller size of Mo compared to Zr results in considerable variation in the bonding. The apical Mo-P distance is much shorter than the basal distances and the Zr-P distances in ZrRuP. The following observations can be summarized: (1) The *M*-P bonds have much larger BO values, indicating a strong covalent character in these alloys due to *M*-P bonding. (2) The apical Mo-P distance (2.438 Å) in *o*-MoRuP is much shorter than the basal Mo-P distances and the Zr-P distances in *o*-ZrRuP. Its BO of 0.196 is significantly larger than the BO of other Mo-P or Zr-P pairs. The three-dimensional *M*-P bonds (Fig. 4) may play a secondary role in superconductivity. (3) The largest BO of *o*-MoRuP is from the Ru-P pairs (0.228 in *o*-MoRuP and 0.243 in *o*-ZrRuP). The latter is larger in spite of the longer bond length (2.453 vs 2.293 Å). This underscores the fact that bonding in these alloys cannot be analyzed simply in terms of bond lengths, but must be based on realistic calculations that fully account for complex interactions of three types of atoms. (4) The role of Mo-Mo and Zr-Zr bonding in these crystals has been speculated in the past.[17] Our calculation shows that the BO between these pairs is relatively small. The BO between Ru-Ru pairs is even smaller. (5) The total crystal BO, which is defined as the summation of all BO in the crystal for atomic pairs with bond lengths less than 3.5 Å, is 6.40 for *o*-MoRuP and 7.46 for *o*-ZrRuP. This indicates that *o*-ZrRuP actually has a stronger covalent bonding character than *o*-MoRuP. This is primarily due to the relatively stronger Ru-Zr bonds.

It should be pointed out that in the past, analysis of crystal structure and bonding were carried out at a very rudimentary level, based only on the number of conduction electrons and the crystal volume or the bond distances. In the present study, the analysis is based on *ab initio* quantum-mechanical calculations, which provide much more reliable results.

TABLE V. Calculated Mulliken effective charges Q^* (electrons) (Ref. 36) of *o*-MoRuP and *o*-ZrRuP.

	o-MoRuP	*o*-ZrRuP
Mo or Zr	5.751	3.330
Ru	8.275	8.529
P	4.974	5.143

TABLE VI. Calculated bond order *o*-MoRuP and *o*-ZrRuP for bond distances of Table III.

	Bond order (electron)			Bond order (electron)	
Atom-atom	$M=$Mo	$M=$Zr	Atom-atom	$M=$Mo	$M=$Zr
Ru-Ru	0.020×2	0.007×2	Ru-P	0.179	0.138
				0.228	0.243
Ru-*M*	0.015	0.103		0.149×2	0.188×2
	0.046×2	0.070×2			
	0.046×2	0.077×2	*M*-*M*	0.052×2	0.061×2
	0.096	0.120		0.038×2	0.053×2
M-P	0.100×2	0.076×2			
	0.048×2	0.100×2			
	0.196	0.124			

IV. COMMENTS AND PERSPECTIVES

In summary, we have reported the structure and x-ray powder diffraction pattern of the orthorhombic superconductor *o*-MoRuP. Based on this structure, first-principles electronic structure calculations were carried out and compared with results of a similar calculation of the isostructural *o*-ZrRuP. Our results indicate that the key elements of the difference in T_c are the different values in the DOS at the Fermi level. It is demonstrated that using structural data alone in past analyses of superconducting properties in many $TT'X$ superconductors is not sufficient. An *ab initio* calculation is necessary for understanding the electronic structure and bonding in these alloys. Further elucidation of the superconducting properties such as the direct evaluation of the transition temperature may require calculations on the lattice dynamics and electron-phonon interactions in these alloys. We plan to determine more precisely the crystal structures of other members of the $TT'X$ family and perform similar electronic structure calculations.[35] It is then possible to have a much clearer pattern on the interrelationship among superconducting properties, crystal structures, and electronic properties in this class of important metallic superconductors. Although the superconducting transition temperatures in the $TT'X$ family are much lower than that of the much celebrated MgB_2 with a $T_c=39.5$ K, the existence of many isostructural members and the possibility of forming solid solutions among them offer a much better opportunity for parameter variations that could result in the further increase of T_c in this class of compounds.

ACKNOWLEDGMENTS

R. Drew is thanked for the superconductivity data measured using a SQUID. Work at UMKC was supported by DOE under Grant No. DE-FG02-84ER45170. Work at NIST was partially supported by ICDD and DOE. Work at BP-Amoco was partially supported by ICDD.

[1] A. Roger, J. P. Sénateur, and R. Fruchart, Ann. Chim. (Paris) **4**, 79 (1969).
[2] R. Fruchart, A. Roger, and J. P. Sénateur, J. Appl. Phys. **40**, 1250 (1969).
[3] Roy-Montreuil, B. Deyris, A. Michel, A. Rouault, A. P. L'Heritier, A. Nylund, J. P. Sénateur, and R. Fruchart, Mater. Res. Bull. **7**, 813 (1972).
[4] V. Johnson and W. Jeitschko, J. Solid State Chem. **4**, 123 (1972).
[5] R. Guvsrin, and M. Sergent, Mater. Res. Bull. **12**, 381 (1977).
[6] J. P. Sénateur, R. Fruchart, D. Boursier, A. Rouault, Roy-Montreuil, and B. Deyris, J. Phys. (Paris), Colloq. **38**, C7-61 (1977).
[7] A. Mewis, Z. Naturforsch. B **34**, 14 (1979).
[8] H. Barz, H. C. Ku, G. P. Meisner, Z. Fisk, and B. T. Matthias, Proc. Natl. Acad. Sci. U.S.A. **77**, 3132 (1980).
[9] G. P. Meisner, H. C. Ku, and H. Barz, Mater. Res. Bull. **18**, 983 (1983).
[10] R. Muller, R. N. Shelton, J. W. Richardson, and R. A. Jacobson, J. Less-Common Met. **92**, 177 (1983).
[11] X.-Z. Wang, B. Chevalier, J. Etourneau, and P. Hagenmuller, Mater. Res. Bull. **20**, 517 (1985).
[12] I. Shirotani, N. Ichihashi, K. Nozawa, M. Kinoshita, T. Yagi, K. Suzuki, and T. Enoki, Jpn. J. Appl. Phys., Suppl. **32–3**, 695 (1993).
[13] I. Shirotani, K. Tachi, K. Takeda, S. Todo, T. Yagi, and K. Kanoda, Phys. Rev. B **52**, 6197 (1995).
[14] I. Shirotani, K. Tachi, N. Ichihashi, T. Adachi, T. Kikegawa, and O. Shimomura, Phys. Lett. A **205**, 77 (1995).
[15] I. Shirotani, M. Hori, K. Tachi, S. Todo, and T. Yagi, J. Alloys Compd. **256**, L1 (1997).
[16] I. Shirotani, Y. Konno, Y. Okada, C. Sekine, S. Todo, and T. Yagi, Solid State Commun. **108[12]**, 967 (1998).
[17] I. Shirotani, M. Takeya, I. Kaneko, C. Sekine, and T. Yagi, Solid State Commun. **116**, 683 (2000).
[18] I. Shirotani, M. Takeya, I. Kaneko, C. Sekine, and T. Yagi, Physica C **357**, 329 (2001).
[19] Powder Diffraction File (PDF), produced by International Centre for Diffraction Data (ICDD), 12 Campus Blvd., Newtown

Square PA 19073-3273.
[20] H. M. Rietveld, J. Appl. Crystallogr. **2**, 65 (1969).
[21] R. A. Young, *The Rietveld Method*, International Union of Crystallography Monograph (Oxford Science, Oxford, 1995).
[22] R. B. Von Dreele, and A. C. Larson, *GSAS, The General Structure Analysis System* (Los Alamos National Laboratory, which is operated by the University of California for the U.S. Department of Energy, 2002), through U.S. DOE Contract No. W-7405-ENG-36.
[23] D. K. Seo, J. Q. Ren, M.-H. Whangbo, E. Canadell, Inorg. Chem. **36**, 6058 (1997).
[24] I. Shirotani, Mol. Cryst. Liq. Cryst. **86**, 1943 (1982).
[25] Toth Information Systems, Inc., CRYSTMET—The Metals Database, Version 1.20 (2001).
[26] I. D. Brown, ''Accumulated Table of Bond Valence Parameters,'' http://ccp14.semo.edu/ccp/web-mirrors/i-d-brown/bond-valence-param/bvparm.cif
[27] W. Y. Ching, J. Am. Ceram. Soc. **73**, 3135 (1990).
[28] W. Y. Ching, Y.-N. Xu, G. Zhao, K. W. Wong, and F. Zandiehnadem, Phys. Rev. Lett. **59**, 1333 (1987).
[29] G.-L. Zhao, Y.-N. Xu, W. Y. Ching, and K. W. Wong, Phys. Rev. B **36**, 7203 (1987).
[30] W. Y. Ching, M.-Z. Huang, Y.-N. Xu, W. G. Harter, and F. T. Chan, Phys. Rev. Lett. **67**, 2045 (1991).
[31] M.-Z. Huang, Y.-N. Xu, and W. Y. Ching, Phys. Rev. B **46**, 6572 (1992).
[32] Y.-N. Xu, W. Y. Ching, Y. Lou, and Y. C. Jean, Phys. Rev. B **52**, 12 946 (1995).
[33] W. Y. Ching, Y.-N. Xu, Y. Lou, and Y. C. Jean, Phys. Rev. B **55**, 2780 (1997).
[34] W. Y. Ching, Y.-N. Xu, L. Ouyang, and W. Wong-Ng, J. Appl. Phys. (to be published).
[35] W. L. McMillan, Phys. Rev. **167**, 331 (1968).
[36] R. S. Mulliken, J. Chem. Phys. **23**, 1833 (1955); **23**, 1841 (1955).
[37] Certain commercial equipment, instruments, or materials are identified in this paper in order to specify the experimental procedure adequately. Such identification is not intended to imply recommendation or endorsement by the National Institute of Standards and Technology, nor is it intended to imply that the materials or equipment identified are necessarily the best available for the purpose.